RSC Advances

ROYAL SOCIETY OF CHEMISTRY

www.rsc.org/advances

Influence of particle size and interfacial interactions on the physical and mechanical properties of particle-filled myofibrillar protein gels

Andrew J. Gravelle, Shai Barbut and Alejandro G. Marangoni*

Department of Food Science, University of Guelph, Guelph, ON, Canada

*E-mail: amarango@uoguelph.ca

Abbreviations

IPF – interfacial protein film; RE – recoverable energy; RBX – rice bran wax; SEM – scanning electron microscopy; WI – whiteness index

Key words

Gelation; Myofibrillar gel; particle-filled gel; composite; large deformation; modulus; viscoelastic

Abstract

The physical and mechanical properties of particle-filled composite gels are influenced by a variety of factors which are often system-specific. Here, we report on the effect of solid fillers of varying sizes and surface properties in a model gel system; heat-set comminuted meat protein gels. Hydrophobic rice bran wax particles and hydrophilic glass beads were selected for their contrasting surface chemistry, which influenced the particle/gel interfacial interactions. All composites were found to be stable up to 0.5 volume fraction filler, based on post-gelation liquid loss, light microscopy, and cryo-SEM analyses. The influence of the dispersed particles on the large deformation mechanical properties of the composites were evaluated based on particle type, size, and volume fraction of filler. The behavior of the Young's modulus was compared to that predicted by particle reinforcement theories proposed by van der Poel and Kerner, each with subsequent extensions. Both filler type and size were found to

influence the Young's modulus and stress at 50 % strain. The recoverable energy and post-compression height recovery were found to be predominantly influenced by the filler volume fraction, and were less influenced by particle/gel interactions. Interestingly, filler type and size range were found to have no effect on the cohesiveness of the composites, as this parameter was found to be solely dependent on the volume fraction of the extensible continuous phase. The influence of filler on the optical properties of the composites were evaluated by reflectance spectroscopy in the visible range, and interpreted based on the effect of the filler optical properties. The results from this study indicate that filler size, surface chemistry, and incorporation level can strongly influence the macroscopic physical characteristics of heat-induced comminuted myofibrillar protein composite gel systems.

1. Introduction

Particulate-reinforced composite materials are utilized in a variety of applications across a broad range of fields, such as in the production of cement and other construction materials, and reinforced rubbers and plastics. The addition of filler particles to a continuous matrix can induce a variety of desirable traits such as resistance to compression,[1] an increase in shear and elastic moduli,[2-5] and a higher fracture stress.[6, 7] The effect of such fillers on the large deformation properties of particle-filled soft solids depends on a variety of system-specific parameters. These include i) the mechanical properties of the continuous matrix, ii) the physical and mechanical properties of the filler, such as shape, orientation, volume fraction, and mechanical strength, and iii) the extent of filler/matrix interactions.[8] For example, particles having a high affinity for the matrix (i.e., bound or active fillers) generally increase the strength of a composite material.[9] The extent of this effect is also dictated by the modulus of the filler relative to that of the matrix, as a higher modulus will produce a greater effect. Conversely, unbound or inactive fillers have little or no interaction with the continuous phase, resulting in a weaker structure.

The influence of a dispersed phase on the mechanical attributes of a composite material is of particular relevance to food systems, as many food matrices can be described as a complex mixture of biomaterials which form a continuous gel matrix containing particulate inclusions.[3, 10, 11] In such systems, the large-deformation mechanical properties of these composite materials will also impact textural attributes and sensory perception. In this regard, particle-filled protein gels,[12, 13] and particularly emulsion-filled gels have received notable attention.[3, 9, 14, 15] The influence of these fillers is relatively complex, as the dispersed phase generally consists of liquid droplets stabilized by emulsifiers which can be selected to either promote or hinder filler/matrix interactions. In addition, these systems can be further complicated by several factors. For example, the modulus of the dispersed phase is directly related to the particle diameter, and can also be influenced by the formation of an interfacial film. Additionally, flocculation of the filler particles during gelation can influence both the available surface area for filler/matrix interactions and the effective volume the particles occupy.[3]

In contrast, the role of fillers in meat protein gels has primarily been addressed using a more empirical approach, where the influence of fillers has been interpreted through evaluation of stability, microstructure, and mechanical properties.[16, 17] In the present work, we have approached this type of system as a model particle-filled protein gel to assess the influence of matrix/filler interactions, as well as the effect of size and volume fraction of the dispersed particles. Finely comminuted meat protein gels are non-reversible, thermally induced gels prepared from muscle tissue. The formation of these highly elastic soft materials requires extensive comminution under saline conditions to facilitate the extraction of salt-soluble myofibrillar proteins.[18] During thermal treatment, these proteins (predominantly myofibrillar proteins) undergo a series of reorganization processes which occur over distinct temperature ranges.[19, 20] The first phase of gel formation occurs between 30 and 50 °C, and involves denaturation and aggregation of the globular heavy meromyosin head-groups.[21] Further heating induces the denaturation of the helical light meromyosin tail-groups, resulting in hydrophobic protein/protein

interactions between the aggregates, giving rise to the continuous gel network. This type of system is most commonly encountered in certain food products such as frankfurter and bologna-style products, in which a fat phase is incorporated during the comminution stage. The resulting fat particles are on the order of 10 μm to >100 μm, and become bound to the protein matrix during gelation, thus forming a composite material often referred to as a meat emulsion, despite not fitting the strict definition of a true emulsion.[22] Due to the inherently complex nature of this system, the exact mechanism of fat stabilization is not fully understood, however it is generally accepted that the dispersed fat globules are bound to the bulk protein gel via the formation of an interfacial protein film (IPF).[22, 23] It has been proposed that this interfacial layer is formed by the preferential assembly of the heavy meromyosin head-groups at the surface of the fat globules during the initial stages of thermal treatment, analogous to the agglomeration of myosin molecules discussed above. Further heating integrates these protein-coated fat droplets into the gel network, thus binding the dispersed fat phase into the bulk gel as a 'bound' or 'active' filler.

Here we have used two model fillers with contrasting surface chemistries; hydrophobic wax particles and hydrophilic glass beads. The purpose of this work was to determine the effect of these fillers on the stability, structure, and physical and mechanical properties of these composite materials as a function of filler type, size, and volume fraction.

2. Materials & Methods

2.1. Materials

Twenty kg of fresh boneless, skinless chicken breast meat was purchased from a national supermarket (Kirkland Signature, Costco Wholesale Canada Ltd., Ottawa, ON). Within 48 hrs of purchasing, all visible fat and connective tissue was removed and the meat was chopped in a bowl chopper (Schneidmeister SMK 40, Berlin, Germany) at the low speed setting for approximately 30 sec and incorporated by hand

to produce a homogeneous mixture. The meat was then separated into ~750 g batches in polyethylene bags, vacuum packed and stored at -20 °C until used. Protein content of the meat was determined to be 21.91 ± 0.43 % using the Dumas method and a nitrogen conversion factor of 5.53.[24]

Two types of filler particles were obtained to be used as rigid fillers with contrasting surface properties; rice bran wax (RBX) and glass beads. RBX was selected as a filler with a hydrophobic surface chemistry and because of its relatively high melting point of 78 – 80 °C,[25] which would therefore remain in the solid form throughout the thermally-induced protein gelation process (heated to 72 °C; see below). Glass beads were selected for their hydrophilic surface and were therefore anticipated to behave as a passive, unbound filler in the gel network. Glass beads (recycled soda-lime glass Ballotini Impact Beads, Potters Industries LLC, Valley Forge, PA, USA) were purchased in four size ranges: 0.045-0.090 mm, 0.15-0.21 mm, 0.425-0.60 mm, and 1.0-1.4 mm. The size range of the 0.425-0.60 mm particles was reduced to 0.50-0.60 mm through the use of wire-mesh sieves (Haver & Boecker via Fisher Scientific, Ottawa, ON). RBX was purchased in pelletized form (Koster Keunen Inc. via Unipex Solutions Canada, Mississauga, ON) and subsequently chopped in a household chopper/grinder (Cuisinart Mini-Prep Plus, Woodbridge, ON). The particles were then passed through a series of wire mesh sieves to obtain the desired particle size ranges. Due to static build-up, narrow ranges of smaller particle were difficult to obtain. Therefore, three size ranges of RBX were collected: < 0.50 mm, 0.50-0.60 mm, and 1.0-1.4 mm. A visual comparison of the particles is presented in the supplementary material (Figure S1).

2.2. Methods

2.2.1. Preparation of comminuted meat protein gels

After storage, the frozen, homogenized meat was defrosted in chilled water and subsequently inspected for any connective tissue, which were removed with tweezers. All comminuted meat mixtures were prepared using 100 g poultry meat, 50 g water, and 3.75 g salt (2.5% NaCl; Fisher Scientific), giving a final

protein content of ~14.25%. Briefly, the meat emulsions were prepared according to the following protocol: In a household food processor (Braun Household, Germany) 100 g poultry meat was chopped for 60 sec, followed by adding 50 g of water and chopping for 10 sec, then adding 3.75 g of sodium chloride and chopping for an additional 10 sec. The chopping unit was then transferred to an ice bath for 2 min to allow for the extraction of salt-soluble proteins before a final chopping period of 80 sec. The mixture was scraped off the walls of the food processor at regular intervals throughout the preparation procedure to ensure the mixture was chopped homogeneously. Filler particles were added post-chopping to ensure the size of the particles remained unchanged, as well as to avoid damaging the chopping blades. Particles were mixed into the continuous phase by hand using a spatula until a homogeneous mix was obtained, and subsequently chilled for a minimum of one hour prior to thermal treatment. The amount of particles incorporated was based on the 150 g meat/water mixture, on a volume fraction basis. All formulations were prepared in three independent replicates.

After chilling at 4 °C, the raw mixtures were stuffed into 50 ml polypropylene centrifuge tubes (Fisher Scientific) and centrifuged (Model 225, Fisher Scientific) at the low speed setting for 30 sec to remove air pockets. Each tube was stuffed with ~30-35 ml of raw composite. Samples were then heated in a water bath (Haake W-26, Haake, Berlin, Germany) to a core temperature of 72 °C, over approximately 1.5 hr. Core temperature was monitored using a thermocouple unit (Fluke Co. Inc., Model # 52 K/J, Everett, WA) fed through a rubber stopper. Once the desired temperature was reached, the samples were transferred to an ice bath for a short time to arrest the heating process.

2.2.2. Liquid loss

After cooling, liquid which had been expelled from the gels during thermal treatment was drained and measured. Liquid loss was expressed as the ratio of collected fluid relative to the original mass of the continuous phase; *i.e.* the mass of the composite, less the filler component (wt% liquid loss).

144

2.2.3. Reflectance spectroscopy

146 Evaluation of optical properties was performed on three fresh cut cross-sections from each sample with a colorimeter (Mini Scan MS/S, Hunter Lab., Reston, VA) using a 10° standard observer and the D65 illuminant setting. Measurements were repeated three times for each cross section and color was expressed in accordance with the Commission International de l'Eclairage (CIE) system and converted from CIE L*, a*, and b* values[26] to a Whiteness Index (WI), using the following equation:[27-29]

$$WI = 100 - \left[(100 - L^*)^2 + (a^*)^2 + (b^*)^2\right]^{0.5} \quad (1)$$

152

2.2.4. Evaluation of mechanical properties

154 The mechanical properties of the particle-filled composites were evaluated using a two cycle uniaxial compression test.[30] For each sample, a minimum of six cylindrical cores (height: 10 mm; diameter: 15 mm) were compressed between two parallel plates to a strain of 50 % using a texture analyzer (Model TA.XT2 , Stable Micro Systems, Texture Technologies Corp., Scarsdale, NY) outfitted with a 30 kg load cell. The crosshead speed was fixed at 1.5 mm/s during testing and all composites were tested at room temperature. The true stress at maximum strain (σ_{50}) was calculated according to:

160 $$\sigma_{50} = \frac{F}{A}\left(\frac{H_0}{H}\right) \quad (2)$$

where H_0 is the height of the core prior to deformation, and H and A are the height and cross-sectional area at maximum deformation. Equation 2 accounts for the change in cross-sectional area during compression under the assumption of a constant sample volume and uniform expansion during compression. The Young's modulus was determined using the slope of the linear region in the force-deformation curve at the onset of compression (below 15 % strain).

166 The elastic properties of the composites were characterized as the recovery after the first compression (height recovery), defined as the ratio of the compression distance during cycle two relative to cycle one
168 (Figure 1, L_2/L_1). Cohesiveness, a measure of the material's ability to retain structure upon deformation, was defined as the work required to compress the sample through the second cycle relative to the first
170 (Figure 1, W_2/W_1 where $W_X = W_{Xa} + W_{Xb}$). Finally, the recoverable energy (RE) was defined as the ratio of total work measured during the first decompression relative to the work required to compress the
172 sample to a strain of 50 %.[31] This parameter characterizes the ability of the composite material to recover its original form after deformation (Figure 1, W_{1b}/W_{1a}).

174

INSERT FIGURE 1 HERE.

176

2.2.5. Light and cryo-Scanning Electron Microscopy (cryo-SEM)

178 Light microscopy was performed on samples containing RBX only, as composites containing glass particles could not be successfully sectioned. The staining procedure followed that outlined by Youssef
180 & Barbut.[32] Approximately 3 mm thick discs were sectioned from the cooked myofibrillar gels, encased in a cassette, dehydrated with a series of alcohols (50, 70, 90 and 100 %), fixed in paraffin, sectioned (7-
182 10 µm) and stained with haematoxylin and eosin. Stained specimens were imaged with a digital light microscope (Model MIC-D, Olympus Optical Co, Ltd., Tokyo, Japan).

184 For characterization of microstructure by cryo-SEM, the composites were either fractured prior to cryo-treatment, or freeze-fractured under cryogenic conditions. The former samples were torn apart
186 manually to expose the internal network to investigate the nature of the filler/matrix interfaces. Composites subjected to freeze-fracture were sectioned with a blade and placed in a cylindrical plug of a
188 copper sample holder such that a portion of the specimen protruded above the face of the holder. Samples were fixed to the holder by applying Tissue-Tec O.C.T. Compound (Canemco Supplies, St.

Laurent, QC) and the apparatus was then put under vacuum and plunged into liquid nitrogen slush at -210 °C. Once frozen, samples were transferred under vacuum to a cryo-preparation unit (Emitech K1250X Ashford, Kent, UK). For samples prepared by freeze-fracture, the protruding portion of the specimen was fractured with a blunt wedge to expose the internal structure. All samples were sublimated at -80 °C for 30-60 min to remove excess water and subsequently sputter coated with ~20 nm of gold-palladium. After coating, the samples were transferred under vacuum to the cryo-SEM vacuum chamber (Hitachi S-570, Tokyo, Japan) for imaging. Samples were kept below -120 °C and viewed under an accelerating voltage of 10 kV. Digital images were captured using Quartz PCI Imaging software, version 8 (Quartz Imaging Corp., Vancouver, BC) and saved in TIFF format.

2.2.6. Statistical analysis

Liquid loss, recoverable energy (RE), and whiteness index (WI) were all analysed as a randomised complete block design, in which the trials represented the random effect of blocks. The treatments consisted of 2 particle types, 3 particle sizes and 5 levels of volume fraction filler (ϕ_{filler}) in a complete 3-way factorial arrangement. All calculations were performed using the mixed procedure (SAS 9.4, SAS Institute Inc., Cary, NC, USA). Preliminary investigation indicated the statistical distribution of liquid loss was right-skewed, and therefore liquid loss was log-transformed prior to analysis. The Brown and Forsythe test was also used to compare variances among groups for each variable, and indicated heterogeneous variances across levels of ϕ_{filler} for all variables, as well as among filler size ranges for liquid loss and WI. These were incorporated into the models as appropriate. Linear and quadratic orthogonal polynomial contrasts across levels of ϕ_{filler} were used to detect trends in response variables as ϕ_{filler} increased, and interactions of these with filler type and size were used to detect differences in these trends among groups.

3. Theoretical description of particle-filled composite materials

A number of theoretical approaches have been proposed to describe the effect of the volume fraction filler (ϕ_f) on the small deformation properties of particle-filled composite systems (see cited material and references therein).[2, 8, 33-35] Several of these models which were originally proposed to describe the behavior of the shear storage modulus of such composites can also be adapted to describe the effects of ϕ_f on the Young's modulus. One such model was that originally derived by van der Poel,[36] with subsequent modifications by Smith.[33, 37] This theory describes a continuous medium in which non-deformable particles are suspended at random, so that the composite material is homogeneous and isotropic.[36] In this derivation it is assumed that the particles are tightly bonded to the suspending matrix, spherical on average, and non-interacting. The latter assumption limits the validity of this model to ϕ_f of approximately 0.5, due to maximum packing fraction considerations.[33] Van der Poel's model has been applied to several emulsion-filled systems containing relatively pliant inclusions, with a reasonable degree of success.[3, 11, 38, 39] The exact solution to the modified van der Poel theory, as reported by Smith, takes the form:

$$\alpha X^2 + \beta X + \gamma = 0 \quad (3)$$

where the positive root of X is then equal to $(E_c / E_m) - 1$, and E_c and E_m represent the Young's modulus of the composite and that of the continuous matrix, respectively. It was assumed that like other gel systems, the meat protein gel behaves as an incompressible elastic material, and the Poisson ratio of the matrix was therefore taken to be 0.5.[3, 38] For the case where the Young's modulus of the filler is significantly greater than that of the matrix ($E_f >> E_m$), the coefficients in Equation 3 are given by:

$$\alpha = \left(8P - \phi_f^{7/3} S\right)\left(Q - 3M\phi_f\right) - 126PM\phi_f\left(1 - \phi_f^{2/3}\right)^2 \quad (4a)$$

$$\beta = 17.5P\left(Q - 3M\phi_f\right) - 7.5M\phi_f\left(8P - S\phi_f^{7/3}\right) \quad (4b)$$

$$\gamma = -131.25PM\phi_f \quad (4c)$$

where the subscripts *m* and *f* respectively indicate properties of the matrix and filler, ν denotes the Poisson ratio, and E the Young's modulus. The remaining terms are defined as follows: $M = E_f / E_m$, $P = (7 + 5\nu_f)M + 4(7 - 10\nu_f)$, $Q = (8 - 10\nu_m)M + 7 - 5\nu_m$, and $S = 35(7 + 5\nu_f)M(1 - \nu_m) - P(7 + 5\nu_m)$.

Due to the complexity of this solution, Smith also proposed a second-order approximation which, when neglecting the previously stated assumptions ($E_f << E_m$ and $\nu_m = 0.5$), can be written as:[33]

$$\frac{E_c}{E_m} - 1 = \frac{15(1 - \nu_m)(M - 1)\phi_f}{Q - (8 - 10\nu_m)(M - 1)\phi_f} \quad (5)$$

This equation has been utilized to fit the observed behavior of composite systems containing pliable fillers,[11, 38] however it is worth noting that this solution diverges from the exact form at higher values of M.[33]

A second theoretical model describing the reinforcing effect of filler particles in a continuous matrix was that proposed by Kerner.[40] This derivation was built on the same set of assumptions as those employed by van der Poel, and therefore again becomes invalid at sufficiently high ϕ_f. To address this deficiency, Lewis and Nielsen proposed a modification to the original Kerner equation which utilizes a crowding function, ψ, to address the effect of the maximum packing fraction of filler particles, ϕ_{max}.[2] The modified Kerner equation describing the Young's modulus of the composite system relative to that of the unfilled matrix can be written as:

$$\frac{E_c}{E_m} = \frac{1 + AB\phi_f}{1 - B\psi\phi_f} \quad (6)$$

where A and B are constants given by:

$$A = \frac{7 - 5\nu_m}{8 - 10\nu_m} \qquad B = \frac{(E_f / E_m) - 1}{(E_f / E_m) + A} \quad (7)$$

Lewis and Nielsen proposed two potential crowding functions, and the one most relevant to this work (based on fitting experimental data) takes the form:

$$\psi = 1 - \exp\left(\frac{-\phi_f}{1-\left(\phi_f / \phi_{\max}\right)}\right) \quad (8)$$

In Section 4.3 the suitability of these theories for describing the behaviour of the moduli of the particle-filled protein gels under investigation will be evaluated based on filler type and size. Specifically, a comparison of the solutions provided by Equations 3, 5, and 6 is presented.

4. Results & Discussion

4.1. Microstructure of particle-filled gels

INSERT FIGURE 2 HERE.

The structure of the composite gels containing RBX particles of the various size ranges are shown in Figure 2. In the absence of particles (Figure 2a), the finely comminuted protein gel forms a typical continuous, homogeneous matrix absent of any large muscle fibers.[17] Note that the roughly circular holes present in the matrix are air pockets. Although these pockets may be considered an artifact of the preparation procedure, they are commonly present in such systems due to the extensive comminution necessary to facilitate protein extraction, and the high viscosity of the mixture prior to gelation. Panels (b), (c), and (d) show the structure of the gel containing RBX particles of increasing size; < 0.50 mm, 0.50-0.60 mm, and 1.0-1.4 mm, respectively. In all samples, the wax particles were found to be uniformly distributed throughout the gel matrix, with no visible evidence of aggregation or preferential orientation. The appearance of distinct sharp edges and variability in the morphology of the filler particles suggests they remained in the solid state during the heat-induced formation of the gel matrix

(internal temperature of 72 °C). No evidence of liquification or the formation of fat channels was observed, and no fat expulsion was noted after thermal treatment (see Section 4.2).

INSERT FIGURE 3 HERE.

Figures 3 and 4 demonstrate the difference in matrix/filler interaction in the composite gels containing hydrophobic RBX particles and hydrophilic glass beads, respectively. Representative images of the RBX-filled gels depicted in Figure 3 demonstrate the wax particles were well integrated into the protein matrix. In these samples, the fracture plane extended through both the gel and the wax particles, indicating there is a strong interaction between the two phases, while also providing a cross-sectional view of the matrix/filler interface. At these interfaces, the gel matrix appears to have been separated from the surface of the particles, which is likely an artifact caused by the sublimation process used in the SEM sample preparation procedure, as similar cracks were also apparent in the bulk matrix. However, it is evident that a layer of protein separated from the bulk gel and remains in contact with the hydrophobic wax surface. At higher magnifications, protein filaments can be seen extending from the bulk to the particle surface (Figure 3c), further suggesting there is a strong interaction between the matrix and filler, allowing them to behave as tightly bound active fillers in the composite material. In addition, the presence of the protein layer surrounding these lipid-based particles (such as that seen in Figure 3a) may lend support the theory of an interfacial protein film (IPF) surrounding fat droplets in finely comminuted meat products.[23, 41]

INSERT FIGURE 4 HERE.

In Figure 4a, empty semi-spherical pockets can be seen where glass beads were dislodged from the gel matrix as a result of the freeze-fracture process. The smooth appearance of these voids and the absence of any tearing of the gel at the interface upon removal of the filler suggests the glass beads are only weakly associated with the protein. To avoid removing the glass beads from the gel network, the sample shown in Figures 4b and 4c was fractured prior to cryo-treatment. These images highlight the interface of the gel matrix and the hydrophilic filler; there are portions of the exposed glass beads which have a thin layer of protein on the surface, and fibers can be seen extending from the bulk gel to the surface of the glass, indicating some level of interaction. However, this interaction appears to be quite weak because fracture still occurred adjacent to the plane of the filler. In addition, there are portions of glass which are not coated in protein, and some of the beads are physically separated from the gel, despite the more delicate preparation procedure employed (e.g., Figure 4b, lower left quadrant). Therefore, from this microstructural analysis, it was concluded that the hydrophobic RBX particles and hydrophilic glass beads employed in this study respectively behave as strong and weak active fillers in the finely comminuted meat protein gel system.

4.2. Liquid Loss

A common method to monitor the loss of stability in commercial comminuted meat products is via the quantification of expelled liquid upon heat-induced gelation.[17, 42] In a fat or oil-filled myofibrillar protein gel, greater liquid losses can arise due to the thermally-induced pressure increase of the dispersed phase. This increase in pressure can cause ruptures in the gel matrix, resulting in the coalescence of fat droplets and the formation of exudative channels, and can be attributed to an ineffective lipid/protein ratio.[17] Post-gelation liquid loss of the particle-filled gels is presented in Figure 5 as a function of the wt% liquid expelled relative to the initial mass of the continuous phase (i.e., meat, water, and salt). As stated previously, no fat losses were observed for any formulations. The overall trend observed was a

reduction in water loss with increasing ϕ_f, however it is apparent that the type and size of filler influenced the rate of decline. In the RBX-filled gels, the improvement in water retention may be due to the formation of an organized layer of myofibrillar proteins at the filler surface. However, the overall reduction in liquid expulsion with increasing ϕ_f was not strongly influenced by the particle size (Figure 5a), indicating this effect is not strongly surface area-dependent.

INSERT FIGURE 5 HERE.

In contrast to the RBX-filled composites, there is a more clear effect of particle size on liquid loss in the glass-filled gels. Figure 5b demonstrates that gels containing progressively smaller glass particles were able to retain significantly more water at lower filler concentrations. This effect is likely due to the hydrophilic nature of the glass and the exponential increase in surface area with decreasing particle size. The stronger interaction between the glass filler and the aqueous phase in the gel likely restricts the movement of water during the thermal gelation process. These results therefore suggest the glass particles may help stabilize the water present in the gel which would otherwise be able to migrate throughout the gel network, and lead to increased liquid expulsion. The presence of the glass beads thus effectively increasing the water retention of the composite material due to their hydrophilic nature.

It is worth noting that even at the highest incorporation levels ($\phi_f = 0.5$), none of the formulations exhibited signs of instability, which is in agreement with the observations made by light microscopy (i.e., no evidence of the formation of fluid channels). This is likely due to the fact that the particles employed in this study remained solid throughout the gelation process. In a fat or oil-filled comminuted meat gel, the thermal treatment necessary to induce gelation causes a pressure increase in the space occupied by the filler, which can lead to ruptures at the filler/matrix interface and thus increase fluid loss.[32] This

effect becomes amplified with increasing ϕ_f (lower protein/fat ratio), thus reducing the stability of the composite, however such an effect was not seen in the gels containing dispersed solid filler particles.

4.3. Effect of filler on Young's modulus

The effect of added filler on the Young's modulus of the composite gels is presented in Figure 6. In agreement with the general behavior expected by particle reinforcement theory ,[8] the Young's modulus of both the strongly bound RBX- and weakly bound glass bead-filled gels was positively correlated to ϕ_f. It is also apparent that there is a distinct effect of filler particle size on the extent of reinforcement, particularly at higher ϕ_f, where filler reinforcement is most prominent. In systems containing pliable fillers such as filled emulsions, the particle size distribution will dictate E_f,[3] and will thus influence the theoretically-predicted modulus of the composite (see Section 3, Eqs. 3-5). For rigid, non-pliable fillers ($E_f >> E_m$), currently available theories consider only ϕ_f, and do not account for effects of filler size.[8] This type of effect has been reported in some other composite systems, where an increase in the modulus was reported with decreasing particle diameter at equivalent ϕ_f.[2, 43] However, it is worth noting that this behavior is likely system-dependent, as other investigations have shown no effect of particle size,[44] or where size effects only become relevant for nanoparticle-filled composites.[45] This point will be further addressed below.

The distinct differences in the influence on the Young's modulus of the RBX- and glass-filled protein gels suggests the mechanism by which the two particle types are able to reinforce the composite system may differ. To address this possibility, the experimental data was fit to both van der Poel theory, which only considers the particle/matrix interactions (Eqs. 3 and 5; exact solution and second-order simplification, respectively), and Kerner's method, as modified by Lewis and Nielsen to account for the influence of particle crowding (Eq. 6). It should be noted that the existing literature in which van der Poel theory has been employed, both the exact solution[3, 39] and the simplified form[11, 38] have been used,

however no comment has ever been raised about the choice of this selection. For this reason, we have considered both forms of the equation when fitting experimental data.

Several studies which have utilized the van der Poel model to describe the behavior of emulsion-filled systems have noted that a non-uniform distribution of the dispersed phase can arise due to flocculation of the filler particles during gel setting. It has been argued that this phenomenon would influence the 'effective' filler volume fraction (ϕ_{eff}) as such aggregated particles would have a larger volume than the sum of the constituents.[3, 38, 39] In the present work, incomplete mixing during particle incorporation may have contributed to a non-uniform distribution of the filler particles. To accommodate for this issue, we have introduced a fitting parameter α, such that $\phi_{eff} = \alpha\phi_f$,[3] thus providing an alternative method to account for the possibility of short-range particle-particle interactions. When fitting experimental data to Kerner's modified model (Eq. 6), ϕ_{max} was selected as the fitting parameter, as this term accounts for particle crowding in an explicit manner. The latter choice of parameter is justified by the relatively large size distribution of the fillers, as well as the non-spherical morphology of the RBX particles, both of which would affect the filler packing efficiency (see Figure 2). Both fitting parameters were constrained such that $\alpha \geq 1$ and $\phi_{max} \leq 1$, as values not meeting this criteria have no physical meaning.

Tables 1 and 2 compare the theoretical fits of the RBX- and glass-filled meat protein gels, respectively. Reasonable fits were achieved for most particle size ranges, with the exception of the 1.0-1.4 mm glass beads (Eqs. 3, 5, and 6) and the 0.50-0.60 mm glass beads (Eq. 3), as the imposed constraints were not satisfied. It is worth noting that the second-order simplification to van der Poel theory fit the data approximately as accurately as the exact solution for both types of particles (see Tables 1 and 2); however the values of ϕ_{eff} from the simplified form are significantly higher. This observation agrees with that originally reported by Smith, in which it is shown that the simplified form increasingly diverges from the exact solution with increasing values of M (or E_f/E_m), giving a much lower prediction than the exact solution.[33] It is therefore very important to take this discrepancy into consideration, as it has previously

been observed that in some cases even the exact solution has been seen to predict values lower than those observed experimentally.[3, 39] Such an oversight could also severely alter the reported ϕ_{eff}, which may potentially be used to give an indication of the extent of filler aggregation.

Filler size range	van der Poel – exact (Eq. 3)		van der Poel – simplified (Eq. 5)		Lewis & Nielsen (Eq. 6)	
	A	R^2	α	R^2	ϕ_{max}	R^2
< 0.50 mm	1.19	0.94	1.77	0.95	0.63	0.83
0.50-0.60 mm	1.14	0.95	1.70	0.96	0.65	0.91
1.0-1.4 mm	1.05	0.99	1.56	0.99	0.70	0.98

Table 1. Evaluation of theoretical fits for rice bran wax-filled meat protein composite gels. The following assumptions were used: $v_m = 0.5$, $v_f = 0.25$, $E_m = 163.654$ Pa (experimentally determined), $E_f = 60$ GPa.

Filler size range	van der Poel – exact (Eq. 3)		van der Poel – simplified (Eq. 5)		Lewis & Nielsen (Eq. 6)	
	α	R^2	α	R^2	ϕ_{max}	R^2
0.045-0.090 mm	1.22	0.99	1.80	0.99	0.62	0.98
0.15-0.21 mm	1.03	0.99	1.52	0.97	0.71	0.99
0.50-0.60 mm	*dnc	---	1.24	0.99	0.92	0.97
1.0-1.4 mm	*dnc	---	*dnc	---	*dnc	---

*Table 2. Evaluation of theoretical fits for glass bead-filled meat protein composite gels. *dnc indicates the function did not converge within the imposed constraints ($\alpha \geq 1$, $\phi_{max} \leq 1$). The following assumptions were used: $v_m = 0.5$, $v_f = 0.25$, $E_m = 163.654$ Pa (experimentally determined), $E_f = 73$ GPa.*

The behavior of E_c for the RBX-filled gels was modelled fairly accurately by the exact solution to van der Poel theory (Eq. 3), particularly for the larger particles. The decline in goodness of fit with decreasing filler size may be at least partially attributed to the divergence from the assumption of particle sphericity (Fig. 2). A similar trend is seen when using the model proposed by Lewis and Nielsen, however, for the 0.50-0.60 mm and < 0.50 mm size ranges, these fits severely under-predict the observed reinforcement at lower ϕ_f, and is reflected in the poor correlation coefficients. This observation is likely influenced by

the irregular morphology of the filler particles: although the bulk density of these particles would be expected to increase with decreasing particle size, when suspended in a viscous medium, the packing efficiency will be reduced (see Fig. 2). The observed dependence of E_c on filler size, combined with previous evidence of an interfacial protein film at the protein/lipid interface further suggests there is a strong interaction between the protein matrix and the dispersed wax filler. Therefore, the observed reinforcement may also be coupled to the available filler surface area, as this will dictate the efficiency of the interfacial interaction. Additionally, filler shape has been shown to have a clear influence on the relative shear moduli of particle-filled composite gelatin gels,[46] however this effect was predominantly attributed to differences in ϕ_{max}, and less-so to filler size. In the present work, the strong interfacial bond between the RBX filler and gel matrix suggests that both the surface area and filler morphology/packing efficiency may contribute to the greater reinforcement at lower ϕ_f, which cannot be accounted for by either theory considered here.

INSERT FIGURE 6 HERE.

Moduli data of the glass bead-filled gels were fit relatively well by both theories, however with increasing particle size, van der Poel theory required values of $\phi_{eff} < 1$, indicating the experimental data is lower than the theoretical prediction. Since $\phi_{eff} < 1$ is not a physically obtainable value, we conclude the exact solution to van der Poel's equation is not suitable for describing composites containing weakly bound filler particles above a certain size threshold. As noted above, the simplified form of this model (Eq. 5) grossly underestimates the relative modulus for the present system (where $E_f >> E_m$), these solutions were therefore also rejected. In contrast, the modified Kerner equation (Eq. 6) produced reasonable fits for all but the largest glass particles (1.0-1.4 mm), but required larger values for ϕ_{max} with increasing filler size. Interestingly, the value provided for the smallest size range is in close agreement

with the maximum packing fraction for the random packing of uniform spheres (~0.64). Additionally, the size distribution of the glass beads used here also increased with increasing particle diameter. This would be expected to increase the bulk density and thus the packing efficiency, resulting in a larger ϕ_{max}. It can therefore not be ruled out that the particle size distribution may also have influenced the maximum packing fraction value obtained from Eq. 6. However, as discussed above, there may be a surface-area dependent contribution to the observed reinforcement which would also influence the parameters obtained from this model. Since the efficiency of the protein-glass adhesion is unknown, it would be difficult to infer how this interaction would influence the parameter estimates. Regardless of this, with the exception of the 1.0-1.4 mm glass beads, the behavior of the Young's modulus is in good agreement with that predicted by the modified Kerner equation, despite the filler particles being weakly bound to the gel matrix.

A more accurate fit, particularly for the RBX-filled composites, was achieved using a phenomenological power law function of the form:

$$E_c / E_m = \gamma \phi_m^{\ \mu} \quad (9)$$

where the scaling factor μ is given by the slope of the linear fit to the log-log transformed data (Figs. 6c and 6d), which was seen to increase with decreasing particle size. This equation has been written as a function of ϕ_m so as to avoid the asymptote in the transformed data when ϕ_f=0. The fitted data for both the RBX- and glass-filled gels is displayed in Figures 6c and 6d, respectively and the extracted parameters and Pearson correlation coefficients are presented in Table 3. Positive scaling factors were obtained by using $|\ln\phi_m|$ to preserve the trend of increasing E_c with ϕ_f. This type of scaling behavior has also been observed in particle gels and has been interpreted using fractal theory.[47-50] However, it would be difficult to justify the applicability of fractal theory to the present system, considering the large size of the dispersed fillers. Although the intermediate size ranges of glass beads also fit relatively well to this phenomenological model, both the smallest and largest sizes did not (see Fig. 6d, and Table 3).

Particle type	Particle size range	γ	μ	R^2
RBX	< 0.50 mm	0.962	4.35 ± 0.07	1.0
	0.50-0.60 mm	0.937	3.88 ± 0.14	0.98
	1.0-1.4 mm	1.02	3.18 ± 0.09	0.99
Glass	0.045-0.090 mm	0.668	4.68 ± 0.37	0.93
	0.15-0.21 mm	0.890	3.18 ± 0.16	0.97
	0.50-0.60 mm	1.10	2.26 ± 0.11	0.97
	1.0-1.4 mm	1.16	1.04 ± 0.15	0.70

Table 3. Parameters extracted from Eq. 9 by fitting the Young's modulus as a function of volume fraction filler for the particle-filled comminuted meat protein gels (see Figures 6c and 6d).

4.4. Effect of filler on stress at 50 % strain (σ_{50})

In Figure 7, the σ_{50} is shown as a function of ϕ_f. The stress behavior of the strongly bound RBX-filled gels was quite similar to that observed for the modulus, likely due to the highly elastic nature of these gels, which resulted in a nearly continuous linear increase from the onset of compression to σ_{50} (see Fig. 1). As noted in the discussion above for E_c, the significant increase in σ_{50} with decreasing particle diameter is also likely due in part to both the greater surface area available for interaction with the gel matrix and the decreased packing efficiency resulting from their increasingly random morphology. The progressive loss of positive reinforcement on σ_{50} with increasing particle diameter would again be anticipated based on the less extensive protein/lipid interfacial interactions. The larger particles may also begin to surpass the intrinsic defect length of the gel, and will thus act as discontinuities in the matrix.[15] This will result in local stress concentrations near the filler/matrix interface, which may exceed either the interfacial bonds or the bonds supporting the gel structure, leading to the nucleation of fractures.[31, 34, 51] In contrast, the smaller particles allow for a more homogeneous distribution of filler mass, greatly increasing the extent of filler/matrix interactions, and causing less interfacial stress. Therefore, the extensive particle/filler interactions of the smaller RBX fillers, coupled with the strong interfacial adhesion result in an elevated σ_{50} while maintaining structural integrity to a greater extent.

INSERT FIGURE 7 HERE.

In the weakly bound glass-filled composites, the effect of increasing ϕ_f is quite different than that produced by their strongly bound counterparts. Once again, there was a negative correlation between particle size and σ_{50} at higher filler content (ϕ_f>0.33). It should also be noted that a prominent stress fracture event occurred below σ_{50} for all samples prepared with ϕ_f = 0.5 and the observed stress at fracture in these samples decreased with particle size (data not shown). This would further contribute to the weakening of the gel, since the larger particles act as stress concentration points, causing these composites to fracture at a lower strain, and therefore do not build up as high a stress as the gels containing smaller particles. Irrespective of this, above ϕ_f of 0.33 there is a significant increase in σ_{50} from that of the unfilled gel in the composites containing the smaller diameter glass beads (0.045-0.090 mm and 0.15-0.21 mm). There is a modest increase in σ_{50} for the 0.50-0.60 mm particles up to ϕ_f = 0.33; however, above this level we see a reversal of this trend.

Finally, the largest particles show no significant increase in σ_{50} from the control gel at any incorporation level. Taken together, these results further indicate the larger filler particles likely behave more as defects in the gel matrix. This effect is also compounded by the weak interfacial bond, which will lead to debonding at the interface. This will enhance the stress concentration effect,[34] leading to crack formation in the continuous phase, thus reducing the ability of the gel to withstand strain and resulting in a reduction in the σ_{50} relative to the gels containing strongly bound filler. These results demonstrate that both filler size and interfacial interaction strongly affect the influence of the filler particles on the large deformation mechanical properties of finely comminuted meat protein gels.

4.5. Effect of filler on relative recoverable energy, height recovery, and cohesiveness

The relative recoverable energy (RE) gives an indication of the viscoelastic nature of the composite gels. Whereas a perfectly elastic material would exhibit complete energy recovery upon decompression, the viscous component will cause a loss of some of this energy. The more viscous the material, the greater this loss will be. Fig. 8 demonstrates that upon addition of rigid filler particles, the resulting composites become more viscous than the unfilled gel, irrespective of the particle type. In the glass-filled gels, there is no significant effect of particle size, suggesting that due to both the weak interaction between the matrix and filler and the non-deformable nature of the glass, the loss of energy upon compression is solely a function of the amount of elastic material present (ϕ_m). One possible explanation for this phenomenon is that the deformation event dissociates the glass beads from the gel, and as a result the interfacial bonds do not significantly contribute to the post-deformation energy recovery. A similar behavior was exhibited by the RBX-filled gels containing particles in the range of 1.0-1.4 mm. This is a further indication that such large particles exceed the intrinsic defect length of the gel, and as such, they interrupt the continuity of the gel matrix, resulting in deleterious effects on the mechanical behavior of the composite material.[31, 51] In the RBX composites containing smaller filler particles, a significant decrease in RE relative to the pure gel ($\phi_f = 0$) is still observed; however, with increasing ϕ_f the continued loss of RE is arrested. At the highest incorporation level investigated ($\phi_f = 0.5$) there is a clear dependence on the filler size seen in the amount of energy dissipated during compression. The use of smaller particles facilitates a more homogeneous distribution of the filler mass throughout the gel, disrupting the matrix to a lesser extent, thus maximizing particle/gel interactions. This results in a composite material which is more rigid in nature, and effectively reduces the apparent viscosity of the material relative to the gels prepared with larger bound filler particles.

INSERT FIGURE 8 HERE.

The post-deformation height recovery is presented in Figures 8c and 8d. The large recovery exhibited in the absence of any filler (0.937 ± 0.005) demonstrates the inherent elastic nature of the finely comminuted meat protein gels. Figure 8c shows that there is a general decrease in height recovery with increasing ϕ_f (RBX), irrespective of particle size. This behavior indicates that in this composite system which contains strongly bound solid particles, the ϕ_f dictates the macroscopic elastic behavior of the material, despite the more rigid nature of the gels containing smaller particles at higher ϕ_f. The composites containing the weakly bound glass filler also exhibited a reduction in post-deformation height recovery relative to the unfilled gel; however at higher concentrations ($\phi_f > 0.33$) there was a notable effect of particle size resulting in a loss of height recovery. As noted above, the composites having $\phi_f = 0.5$ had a fracture stress below 50% strain, which is likely a major contributing factor for the observed differences in the height recovery of these samples. The stress at fracture was found to increase with decreasing particle size, an effect which was attributed to the increase in surface area, facilitating a more efficient distribution of stress concentration at the filler/gel interface. Therefore, in the weakly bound filler system, we conclude the post-compression height recovery was inversely related to the fracture stress due to a greater number of fracture sites at the particle/gel interface which compromised the integrity of the gels.

The cohesiveness of a material is a measure of its ability to retain its integrity after undergoing stress. In the present study, this property was measured as the work required to deform the sample during the second compression relative to the first. In Figures 8e and 8f, it can be seen that the cohesiveness of the composite gels were negatively correlated to ϕ_f. Interestingly, this same trend was seen for both filler type and size, despite the drastic differences seen in some of the other mechanical properties such as the Young's modulus and σ_{50}. This finding indicates that the behavior of the material over the two cycle compression is consistent, irrespective of the filler characteristics, and the cohesive properties of these composites are predominantly influenced by the amount of elastic material present in the system, i.e.

554 ϕ_m. This result is somewhat surprising, particularly for the higher ϕ_f RBX-filled gels, in that there was a strong filler-size dependence on the Young's moduli of these particle-filled gels, however filler size had
556 no effect on the cohesiveness of these composites. This finding suggests that the elastic nature of the continuous phase plays the predominant role in influencing this particular attribute (see Figure 8a).

558

4.6. Optical properties of particle-filled composite gels

560

INSERT FIGURE 9 HERE.

562

Figure 9 demonstrates the effect of ϕ_f and particle size range on the optical properties of the composite
564 gels. As the meat protein gel was quite pale, the optical traits were evaluated in terms of the Whiteness Index (WI; see Eq. 1). Particle size affects the optical properties of the filler, and the number of particles
566 (scatterers) present will dictate their influence on the WI of the bulk material. The WI of the composites containing optically translucent glass beads were generally found to decrease with increasing ϕ_f, and
568 this effect became more pronounced with increasing particle diameter. This observation can be explained by the refractive properties of the glass filler. With increasing particle size, more light will tend
570 to be diffused into the pocket in which the particle is embedded, reducing the amount of light reflected back to the observer and making the composite appear darker. Conversely, smaller particles have a
572 greater surface curvature, which will have a greater tendency to diffract the incident light to more extreme angles, increasing the odds of the reflected light returning to the observer, and thus appearing
574 lighter. This same phenomenon can be used to explain why the WI of the bulk material (ϕ_f = 1.0) is higher than that of the gel for the smaller particles (0.045-0.090 mm and 0.15-0.21 mm). In the bulk
576 material, the light is scattered throughout a bed of random scatterers, thus increasing the likelihood of being reflected back to the observer. Conversely, when the larger beads are homogeneously distributed

578 throughout the composite, many scattering events result in diffusion into the gel matrix, thus acting as light sinks.

580 In contrast, the RBX-filled composites contain opaque white-to-yellow particles which pale with decreasing particle diameter (see supplementary Fig. S1). A gradual decrease in the WI with ϕ_f was

582 noted for all particle sizes, and this decrease again became more pronounced with increasing particle size. This effect is likely due to a combination of the color of the particles, as well as the rough nature of

584 their surface, which could scatter more light away from the observer. The significantly higher WI of the < 500 µm particles (ϕ_f = 1.0) can be attributed to their physical color and opaque nature (see Fig. S1). The

586 effect of particle size on the WI is not surprising, as the RBX employed in this study had a light yellow color, and when ground to smaller sizes, increased surface roughness which consequently altered the

588 light-scattering properties, resulting in a whiter appearance.

590 **5. Conclusion**

The effects of rigid filler particles dispersed in finely comminuted meat protein gels have been reported.

592 Physical characteristics were evaluated based on filler type (surface characteristics), size range, and ϕ_f. The hydrophobic RBX particles formed a strong interfacial interaction with the protein matrix, while the

594 hydrophilic glass beads had a much weaker interaction, as confirmed by cryo-SEM. No instability was noted in any of the composites prepared up to ϕ_f = 0.50, as determined by post-gelation liquid loss and

596 both light microscopy and cryo-SEM. Water retention increased with ϕ_f, and improved significantly with decreasing particle size, particularly in composites prepared with hydrophilic glass beads. Both E_c and σ_{50}

598 were significantly influenced by filler particle size. The modulus was found to be positively correlated to ϕ_f for all but the largest glass bead fillers (1.0-1.4 mm). The behavior of E_c as a function of ϕ_f was

600 modelled using two established particle reinforcement theories; the van der Poel model with subsequent extensions, and the Kerner equation, modified to account for particle crowding. The RBX-

602 filled composites were best fit by van der Poel theory; however an improved fit was obtained by using a phenomenological power law model. The glass-filled gels were most accurately described by the
604 modified Kerner model, when using ϕ_{max} as the fitting parameter. Filler/matrix interactions were also seen to affect other mechanical properties such as the relative recoverable energy and post-
606 deformation height recovery. In contrast, a decline in cohesiveness with ϕ_f was found to be independent of the filler type or size, and was solely dependent on the content of elastic material (i.e. the continuous
608 phase). The optical scattering characteristics of the composite materials could be interpreted in terms of the optical properties of the filler particles employed. This work highlights the complex role
610 particle/filler interactions play in dictating the mechanical characteristics of particle-filled comminuted meat gels and should provide insight into the mechanisms responsible for these observed effects. These
612 findings should be transferable to other particle-filled soft solids, which have applications in many fields, such as the cosmetic, pharmaceutical, and food industries.

614

Acknowledgements

616 The authors would like to acknowledge the Ontario Ministry of Food and Rural Affairs (OMAFRA) for their financial support. We would also like to thank Dr. Sandy Smith for her assistance with cryo-SEM
618 imaging and Dr. Margaret Quinton for her assistance with the statistical analysis.

620

622 **Figure Captions**

624 *Figure 1. Representative large deformation curve for a two-cycle uniaxial compression to 50 % strain. The composite contained 0.15-0.21 mm glass beads, ϕ_f = 0.33. Denoted areas and lengths were used to*
626 *determine the mechanical properties noted in the text.*

Figure 2. Representative light micrographs of heat-induced rice bran wax (RBX) -filled composite gels prepared using finely comminuted poultry muscle protein as the gelation medium. a) Gel matrix, absent of particles; b) < 0.50 mm RBX particles; c) 0.50-0.60 mm RBX particles; d) 1.0-1.4 mm RBX particles. Samples shown in panels b, c, and d were prepared with ϕ_f = 0.33. White areas represent locations of RBX particles which were removed during the fixation process (or air pockets in some cases). Each micrograph is approximately 3 mm in width.

Figure 3. Cryo-SEM images of heat induced rice bran wax (RBX) -filled composite gels prepared using finely comminuted poultry muscle protein as the gelling medium. RBX appears as the darker region in the upper portion of each panel. Composites were prepared with a particle size range of 0.50-0.60 mm and ϕ_f = 0.33. a) RBX particle embedded in the gel matrix. b) Gel/filler interface showing adhesion of protein to the hydrophobic filler particle where the bulk of the gel has separated from the wax. c) Higher-resolution image of gel/filler interface with visible protein strands extending from the bulk gel to the particle.

Figure 4. Cryo-SEM images of heat induced glass bead-filled composite gels prepared using finely comminuted poultry muscle protein as the gelling medium. a) Empty pockets where weakly bound glass beads were removed from the gel matrix as a result of the freeze-fracture process. Particle size range of 0.15-0.21 mm and ϕ_f = 0.43. b), c) Glass beads embedded in the gel matrix, exposed by gently fracturing the sample prior to cryo-treatment; particle size range 1.0-1.4 mm and ϕ_f = 0.33. In panel c) a thin layer of protein can be seen remaining on sections of the glass inclusions.

Figure 5. Influence of ϕ_f on the liquid loss of heat-set particle-filled comminuted meat protein gels. a) rice bran wax; hydrophobic, strongly bound filler. b) Glass beads; hydrophilic, weakly bound filler. Particle size ranges ●: 1.0-1.4 mm, □: 0.50-0.60 mm, ▲: 0.15-0.21 mm, ◊: 0.045-0.090 mm, ▼: < 0.50 mm.

Figure 6. Effect of filler type, size, and volume fraction filler (ϕ) on the Young's modulus (E_c) of particle-filled comminuted meat protein gels. (a, c) Rice bran wax; strongly bound filler (insets show greater separation in the y-axis). (b, d) Glass beads; weakly bound filler. Experimental data in (a) and (b) were fit to the exact solution of the van der Poel model (Eq. 3) and the Kerner model (Eq. 6), respectively. Fitted parameters are presented in Tables 1 and 2. The data presented in (c) and (d) is a ln-ln transformation of that shown in (a) and (b), respectively. The linear fits correspond to Eq. 9. Note: ϕ_m in panels c and d denote the volume fraction of the gel matrix. Particle size ranges ●: 1.0-1.4 mm, □: 0.50-0.60 mm, ▲: 0.15-0.21 mm, ◊: 0.045-0.090 mm, ▼: < 0.50 mm.

Figure 7. Effect of filler type, size, and volume fraction filler (ϕ) on the Young's modulus (E_c) of particle-filled comminuted meat protein gels. (a) Rice bran wax; strongly bound filler. (b) Glass beads; weakly bound filler. Particle size ranges ●: 1.0-1.4 mm, □: 0.50-0.60 mm, ▲: 0.15-0.21 mm, ◊: 0.045-0.090 mm, ▼: < 0.50 mm.

Figure 8. Effect of filler type, size, and volume fraction filler (ϕ) on (a, b) the relative recoverable energy, (c, d) relative height recovery, and (e, f) cohesiveness of finely comminuted meat protein composite gels with rigid filler particles. (a, c, e) Rice bran wax; strongly bound filler. (b, d, f) Glass beads; weakly bound filler. Particle size ranges ●: 1.0-1.4 mm, □: 0.50-0.60 mm, ▲: 0.15-0.21 mm, ◊: 0.045-0.090 mm, ▼: < 0.50 mm.

674 *Figure 9. Effect of filler type, size, and volume fraction filler (ϕ) on the Whiteness Index of finely comminuted meat composite gels with rigid filler particles. (a) Rice bran wax; strongly bound filler. (b)*
676 *Glass beads; weakly bound filler. (Particle size ranges ●: 1.0-1.4 mm, □: 0.50-0.60 mm, ▲: 0.15-0.21 mm, ◊: 0.045-0.090 mm, ▼: < 0.50 mm).ϕ = 1.0 denotes the bulk filler material.*

678

References

1. Y. Rostamiyan, A. Hamed Mashhadzadeh and A. Salmankhani, *Mater. Design*, 2014, **56**, 1068-1077.
2. T. Lewis and L. Nielsen, *J. Appl. Polym. Sci.*, 1970, **14**, 1449-1471.
3. T. Van Vliet, *Colloid Polym. Sci.*, 1988, **266**, 518-524.
4. J. Nie, B. Du and W. Oppermann, *Macromolecules*, 2005, **38**, 5729-5736.
5. J. Meid, F. Dierkes, J. Cui, R. Messing, A. J. Crosby, A. Schmidt and W. Richtering, *Soft Matter*, 2012, **8**, 4254-4263.
6. K. R. Langley and M. L. Green, *J. Text. Stud.*, 1989, **20**, 191-207.
7. J. M. Manski, I. M. J. Kretzers, S. van Brenk, A. J. van der Groot and R. M. Boom, *Food Hydrocolloid.*, 2007, **21**, 73-84.
8. S. Ahmed and F. R. Jones, *J. Mater. Sci.*, 1990, **25**, 4933-4942.
9. E. Dickinson, *Food Hydrocolloid.*, 2012, **28**, 224-241.
10. K. R. Langley, A. Martin and S. L. Ogin, *Compos. Sci. Technol.*, 1994, **50**, 259-264.
11. P. Rosa, G. Sala, T. van Vliet and F. Van de Velde, *J. Text. Stud.*, 2006, **37**, 516-537.
12. M. Tomczyńska-Mleko, T. Brenner, K. Nishinari, S. Mleko and A. Kramek, *J. Text. Stud.*, 2014, **45**, 344-353.
13. M. Kawecka-Radomska, M. Tomczyńska-Mleko, M. Wesolowska-Trojanowska, K. Kowalczyk, M. Chrząstek and S. Mleko, *Journal of Polymers and the Environment*, 2015, (in press).
14. E. Dickinson and J. Chen, *J. Disper. Sci. Technol.*, 1999, **20**, 197-213.
15. G. Sala, T. van Vliet, M. A. Cohen Stuart, F. van de Velde and G. A. van Aken, *Food Hydrocolloid.*, 2009, **23**, 1853-1863.
16. M. Wu, Y. L. Xiong, J. Chen, X. Tang and G. Zhou, *J. Food Sci.*, 2009, **74**, E207-E217.
17. M. K. Youssef and S. Barbut, *J. Food Sci.*, 2010, **75**, S108-S114.
18. E. Tornberg, *Meat Sci.*, 2005, **70**, 493-508.
19. Y. L. Xiong and C. J. Brekke, *J. Food Sci.*, 1990, **55**, 1540.
20. Y. L. Xiong and C. J. Brekke, *J. Food Sci.*, 1990, **55**, 1544.
21. A. Sharp and G. Offer, *J. Sci. Food Agric.*, 1992, **58**, 63-73.
22. A. Gordon and S. Barbut, *Crit. Rev. Food Sci. Nutr.*, 1992, **32**, 299-332.
23. A. Gordon and S. Barbut, *Canadian Institute of Food Science and Technology Journal*, 1991, **24**, 136-142.
24. F. Mariotti, D. Torné and P. P. Mirand, *Crit. Rev. Food Sci. Nutr.*, 2008, **48**, 177-184.
25. A. Blake, E. D. Co and A. G. Marangoni, *J. Am. Oil Chem. Soc.*, 2014, **91**, 885-903.
26. *Journal*, 1986.
27. H. R. Bolin and C. C. Huxsoll, *J. Food Sci.*, 1991, **56**, 416-418.
28. M. H. Lohman and R. W. Hartel, *J. Am. Oil Chem. Soc.*, 1994, **71**, 267-276.
29. W. Prasert and P. Suwannaporn, *J. Food Eng.*, 2009, **95**, 54-61.
30. M. C. Bourne, *Food Technol.*, 1978, **32**, 62-66.
31. G. Sala, T. van Vliet, M. A. Cohen Stuart, G. A. van Aken and F. van de Velde, *Food Hydrocolloid.*, 2009, **23**, 1381-1393.
32. M. K. Youssef and S. Barbut, *Meat Sci.*, 2009, **82**, 228-233.
33. J. C. Smith, *J. Res. Nat. Bur. Stand.*, 1975, **79A**, 419-423.
34. Y. C. Gao and J. Lelievre, *Polym. Eng. Sci.*, 1994, **34**.
35. R. Pal, *J. Colloid Interf. Sci.*, 2002, **245**, 171-177.
36. C. van der Poel, *Rheol. Acta*, 1958, **1**, 198-205.
37. J. C. Smith, *J. Res. Nat. Bur. Stand.*, 1974, **78A**.
38. J. Chen and E. Dickinson, *J. Text. Stud.*, 1998, **29**, 285-304.

39. K. H. Kim, J. M. S. Renkema and T. Van Vliet, *Food Hydrocolloid.*, 2001, **15**, 295-302.
40. E. H. Kerner, *P. Phys. Soc. Lond. B*, 1956, **69**, 808-813.
41. W. K. Jones, Chicago, IL, 1984.
42. M. Wu, Y. L. Xiong and J. Chen, *Meat Sci.*, 2011, **88**, 384-390.
43. J. Spanoudakis and R. J. Young, *J. Mater. Sci.*, 1984, **19**, 473-486.
44. C. J. R. Verbeek, *Matter. Lett.*, 2003, **57**, 1919-1924.
45. X. L. Ji, J. K. Jing, W. Jiang and B. Z. Jiang, *Polym. Eng. Sci.*, 2002, **42**, 983-993.
46. R. K. Richardson, G. Robinson, S. B. Ross-Murphy and S. Todd, *Polym. Bull.*, 1981, **4**, 541-546.
47. L. G. B. Bremer, T. van Vliet and P. Walstra, *J. Chem. Soc. Farad. T. 1*, 1989, **85**, 3359-3372.
48. W.-H. Shih, W. Y. Shih, S.-I. Kim, J. Lui and I. A. Aksay, *Phys. Rev. A*, 1990, **42**, 4772-4779.
49. R. Vreeker, L. L. Hoekstra, D. C. den Boer and W. G. M. Agterof, *Food Hydrocolloid.*, 1992, **6**, 423-435.
50. M. Stading, M. Langton and A. M. Hermansson, *Food Hydrocolloid.*, 1993, **7**, 195-212.
51. T. Van Vliet, H. Luyten and P. Walstra, in *Food Colloids and Polymers: Stability and Mechanical Properties*, eds. E. Dickinson and P. Walstra, Royal Society of Chemistry, Cambridge, 1993, vol. 113, pp. 175-266.

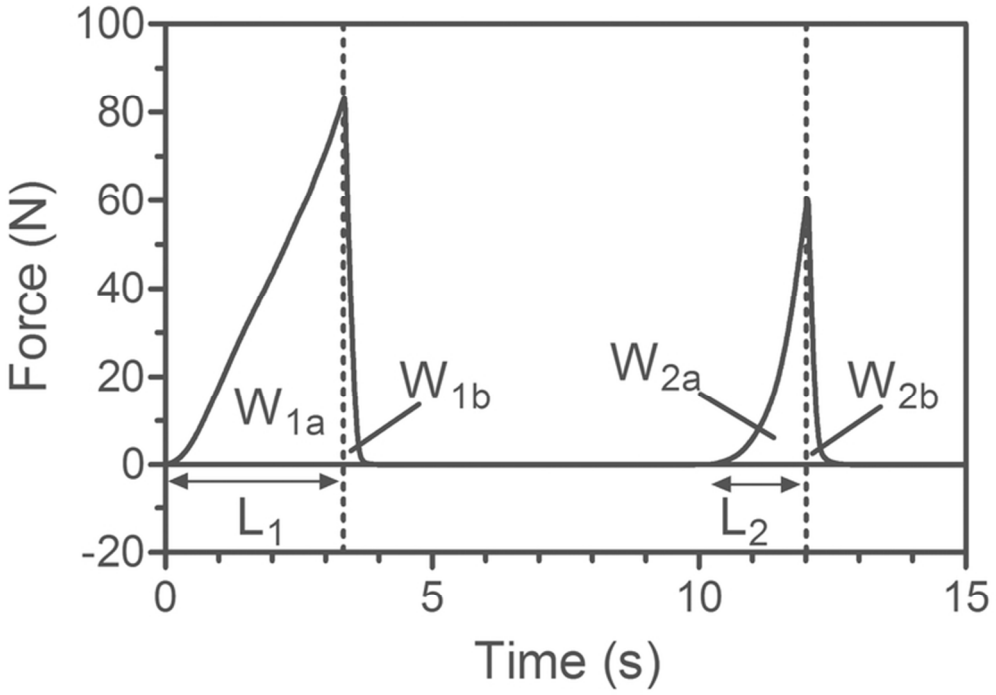

Figure 1. Representative large deformation curve for a two-cycle uniaxial compression to 50 % strain. The composite contained 0.15-0.21 mm glass beads, Φf = 0.33. Denoted areas and lengths were used to determine the mechanical properties noted in the text.
66x46mm (300 x 300 DPI)

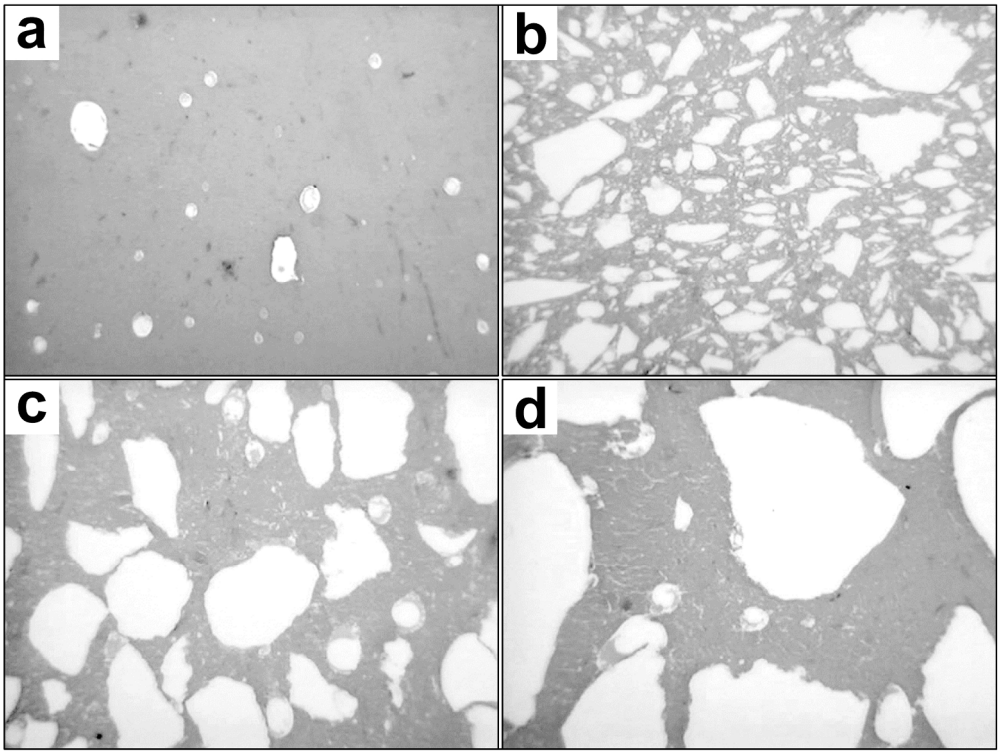

Figure 2. Representative light micrographs of heat-induced rice bran wax (RBX) -filled composite gels prepared using finely comminuted poultry muscle protein as the gelation medium. a) Gel matrix, absent of particles; b) < 0.50 mm RBX particles; c) 0.50-0.60 mm RBX particles; d) 1.0-1.4 mm RBX particles. Samples shown in panels b, c, and d were prepared with Φf = 0.33. White areas represent locations of RBX particles which were removed during the fixation process (or air pockets in some cases). Each micrograph is approximately 3 mm in width.
219x165mm (300 x 300 DPI)

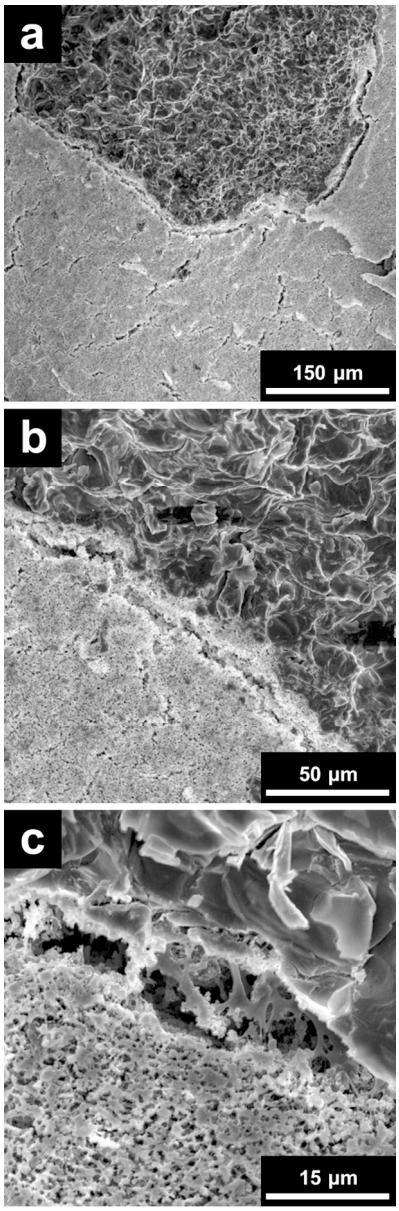

Figure 3. Cryo-SEM images of heat induced rice bran wax (RBX) -filled composite gels prepared using finely comminuted poultry muscle protein as the gelling medium. RBX appears as the darker region in the upper portion of each panel. Composites were prepared with a particle size range of 0.50-0.60 mm and Φf = 0.33. a) RBX particle embedded in the gel matrix. b) Gel/filler interface showing adhesion of protein to the hydrophobic filler particle where the bulk of the gel has separated from the wax. c) Higher-resolution image of gel/filler interface with visible protein strands extending from the bulk gel to the particle.
54x165mm (300 x 300 DPI)

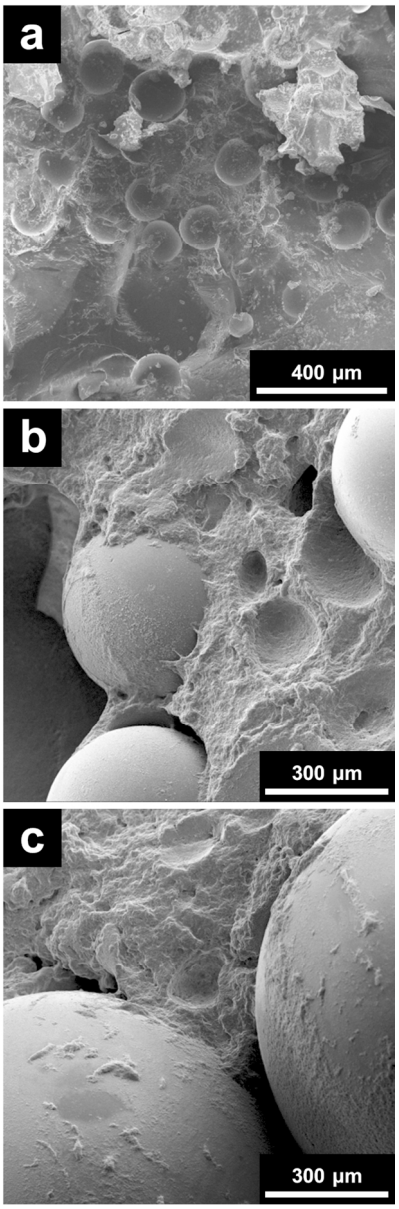

Figure 4. Cryo-SEM images of heat induced glass bead-filled composite gels prepared using finely comminuted poultry muscle protein as the gelling medium. a) Empty pockets where weakly bound glass beads were removed from the gel matrix as a result of the freeze-fracture process. Particle size range of 0.15-0.21 mm and Φf = 0.43. b), c) Glass beads embedded in the gel matrix, exposed by gently fracturing the sample prior to cryo-treatment; particle size range 1.0-1.4 mm and Φf = 0.33. In panel c) a thin layer of protein can be seen remaining on sections of the glass inclusions.
54x166mm (300 x 300 DPI)

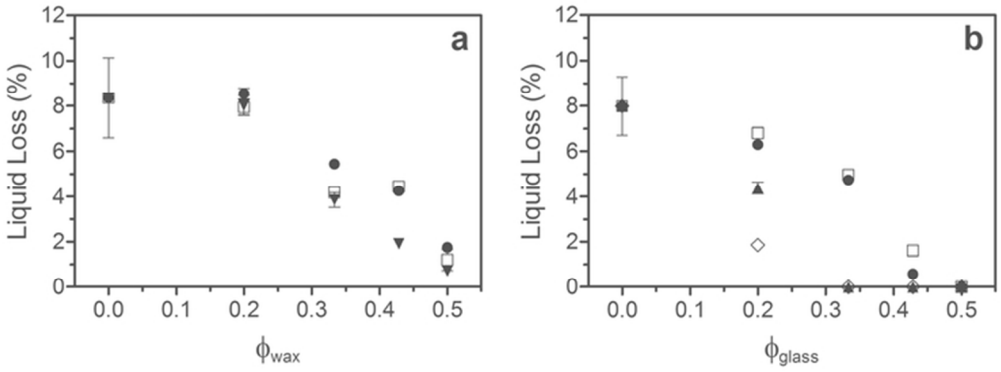

Figure 5. Influence of Φ_f on the liquid loss of heat-set particle-filled comminuted meat protein gels. a) rice bran wax; hydrophobic, strongly bound filler. b) Glass beads; hydrophilic, weakly bound filler. Particle size ranges ●: 1.0-1.4 mm, □: 0.50-0.60 mm, ▲: 0.15-0.21 mm, ◇: 0.045-0.090 mm, ▼: < 0.50 mm.
62x23mm (300 x 300 DPI)

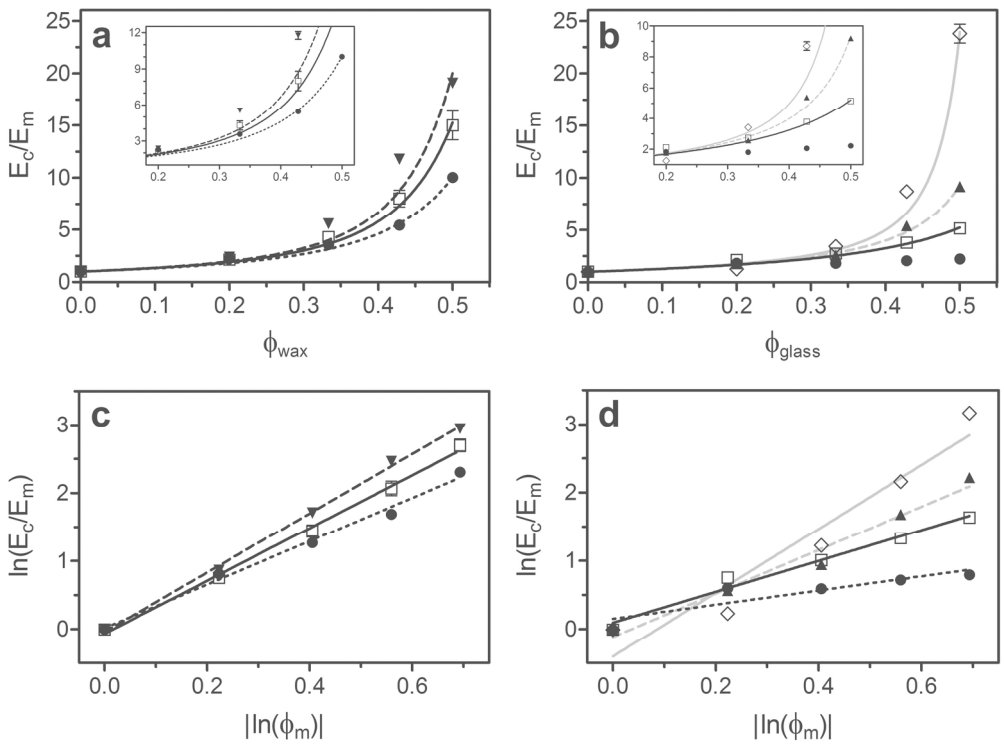

Figure 6. Effect of filler type, size, and volume fraction filler (Φ) on the Young's modulus (Ec) of particle-filled comminuted meat protein gels. (a, c) Rice bran wax; strongly bound filler (insets show greater separation in the y-axis). (b, d) Glass beads; weakly bound filler. Experimental data in (a) and (b) were fit to the exact solution of the van der Poel model (Eq. 3) and the Kerner model (Eq. 6), respectively. Fitted parameters are presented in Tables 1 and 2. The data presented in (c) and (d) is a ln-ln transformation of that shown in (a) and (b), respectively. The linear fits correspond to Eq. 9. Note: Φ_m in panels c and d denote the volume fraction of the gel matrix. Particle size ranges ●: 1.0-1.4 mm, □: 0.50-0.60 mm, ▲: 0.15-0.21 mm, ◇: 0.045-0.090 mm, ▼: < 0.50 mm.
169x125mm (300 x 300 DPI)

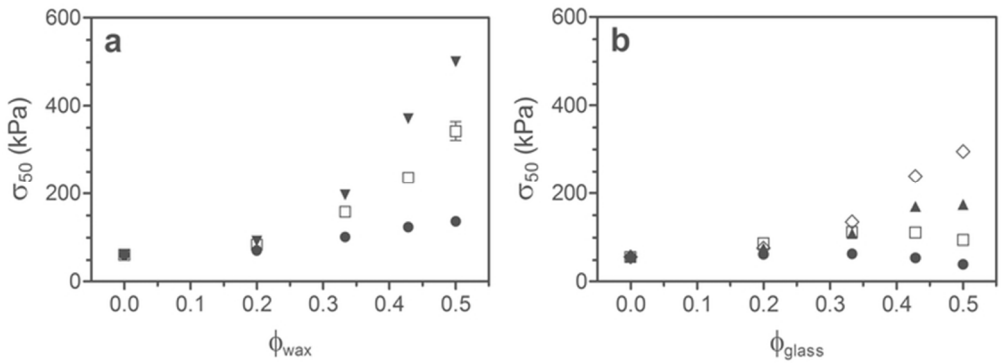

Figure 7. Effect of filler type, size, and volume fraction filler (Φ) on the Young's modulus (Ec) of particle-filled comminuted meat protein gels. (a) Rice bran wax; strongly bound filler. (b) Glass beads; weakly bound filler. Particle size ranges ●: 1.0-1.4 mm, □: 0.50-0.60 mm, ▲: 0.15-0.21 mm, ◇: 0.045-0.090 mm, ▼: < 0.50 mm.
64x23mm (300 x 300 DPI)

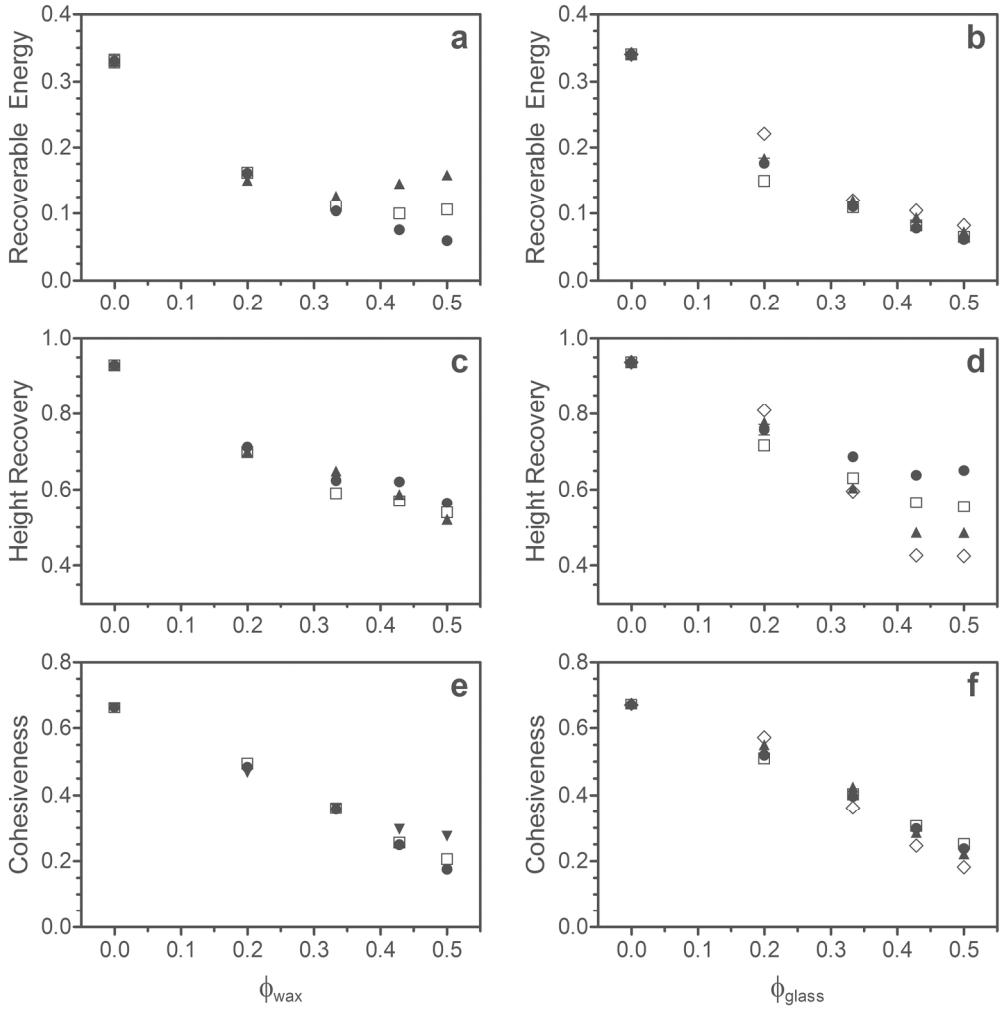

Figure 8. Effect of filler type, size, and volume fraction filler (Φ) on (a, b) the relative recoverable energy, (c, d) relative height recovery, and (e, f) cohesiveness of finely comminuted meat protein composite gels with rigid filler particles. (a, c, e) Rice bran wax; strongly bound filler. (b, d, f) Glass beads; weakly bound filler. Particle size ranges ●: 1.0-1.4 mm, □: 0.50-0.60 mm, ▲: 0.15-0.21 mm, ◇: 0.045-0.090 mm, ▼: < 0.50 mm.
182x184mm (300 x 300 DPI)

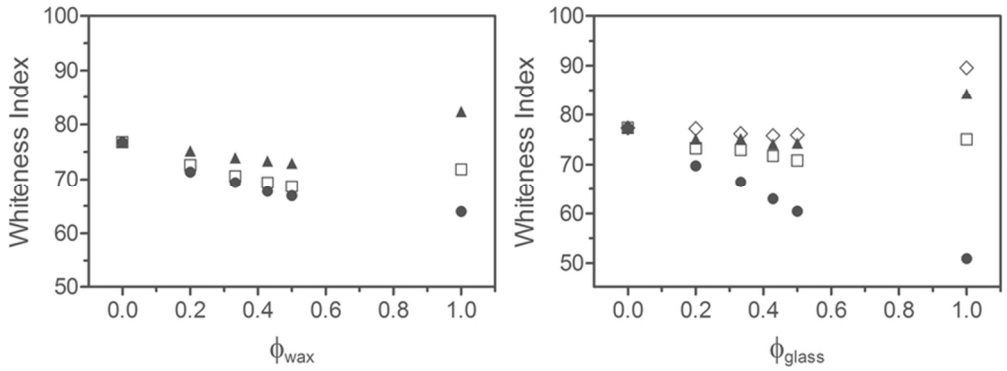

Figure 9. Effect of filler type, size, and volume fraction filler (Φ) on the Whiteness Index of finely comminuted meat composite gels with rigid filler particles. (a) Rice bran wax; strongly bound filler. (b) Glass beads; weakly bound filler. (Particle size ranges ●: 1.0-1.4 mm, □: 0.50-0.60 mm, ▲: 0.15-0.21 mm, ◇: 0.045-0.090 mm, ▼: < 0.50 mm). Φ = 1.0 denotes the bulk filler material.

73x26mm (300 x 300 DPI)